Optical properties of silicon and germanium determined by high-precision analysis of reflection electron energy loss spectroscopy spectra

L. H. Yang,[1] K. Tőkési [ORCID],[2] J. Tóth,[2] B. Da,[3] H. M. Li,[4,*] and Z. J. Ding[1,†]

[1]*Hefei National Laboratory for Physical Sciences at Microscale and Department of Physics, University of Science and Technology of China, Hefei, Anhui 230026, People's Republic of China*
[2]*Institute for Nuclear Research, Hungarian Academy of Sciences (ATOMKI), Debrecen, Hungary*
[3]*Research and Services Division of Materials Data and Integrated System (MaDIS), National Institute for Materials Science (NIMS), 1-2-1 Sengen, Tsukuba, Ibaraki 305-0047, Japan*
[4]*Supercomputing Center, University of Science and Technology of China, Hefei, Anhui 230026, People's Republic of China*

We present a detailed analysis and comparison of four models describing the extension of the electron-energy loss function from the optical limit of $q \rightarrow 0$ into the (q, ω) plane to obtain the bulk and surface terms of differential inverse inelastic mean free paths. We found that the best model that describes accurately and times efficiently the calculation of the energy loss function of free-electron-like materials is the combination of the Penn algorithm [Phys. Rev. B **35**, 482 (1987)] with the Ritchie-Howie method [Philos. Mag. **36**, 463 (1977)]. Applying this model in our reverse Monte Carlo method, we determined, with high-precision, electron-energy loss functions of silicon and germanium based on the theoretical analysis of the high-energy resolution reflected electron energy loss spectroscopy (REELS) spectra, measured at 3, 4, and 5 keV incident electron energies. The refractive index n, the extinction coefficient k, and the complex dielectric function ($\varepsilon = \varepsilon_1 + i\varepsilon_2$) were calculated from the obtained energy loss function in a wide energy loss range of 0–200 eV. The accuracy of the obtained results is justified with various sum rules. We found that the calculated optical data of Si and Ge fulfill the sum rules with an average accuracy of 0.11% or even better. Therefore, the use of these optical data in materials science and surface analysis is highly recommended for further applications.

I. INTRODUCTION

Silicon and germanium remain the key elements in microelectronics. These two materials are applied in some devices [1–3]. Nowadays, they are used as nanometallic memristors [4], photonic devices [5,6], optoelectronic devices [7], and spin-qubit devices [8–10]. More devices are also being developed, indicating the need for better knowledge of the material properties of the elements of these devices. Therefore, in this work, we aim at a revision of the optical properties of silicon and germanium. In recent years, a well-established high-precision technique, based on a combination of the reflection electron energy loss spectroscopy (REELS) measurements and the so-called reversed Monte Carlo (RMC) method [11], was developed to obtain optical constants of elements in a wide range of electron energy loss. The key to obtaining good results by RMC is the high-precision theoretical analysis of the high energy resolution experimental data.

The advantage of the REELS technique compared to the standard optical techniques is that the measurable electron energy loss range of REELS is about 100 eV in one measurement, while optical measurement requires the multilight sources, respective instruments, and measurement methods to cover this wide wavelength range. The REELS spectrum, in general, contains not only the bulk electronic excitation but also the surface excitation [12,13]. For an accurate theoretical modeling of the REELS spectra, we must mimic all possible interactions and experimental conditions with high precision. Most importantly, one must pay special attention to the description of the inelastic cross sections, including the surface and bulk contributions.

Many approaches have been developed and used for the modeling of REELS spectra, where the surface effects were taken into account in various ways in the treatment of electron inelastic scattering during recent decades [14–23]. A dielectric response theory [24,25], in which the experimental optical dielectric data are used to describe the electron-energy loss function (ELF), is the most frequently used theoretical approach for the description of the inelastic scattering processes. The surface excitation probability is related to the position, energy, and moving direction of electrons [20]. Although significant improvements have been made in describing the inelastic cross sections, a good model is still awaiting development. Below, we first review some of the previous models.

Early simulations employed only the bulk ELF. It was found that the calculation can describe the experimental spectra at high primary energies and for large energy losses; however, the approach may yield a large discrepancy at low primary energies and for low energy losses. It was shown

*Author to whom all correspondence should be addressed: hmli@ustc.edu.cn
†zjding@ustc.edu.cn

that the discrepancy is attributed to the fact that the optical ELF does not contain the information of surface excitations [26]. To improve the description of the inelastic cross section and extract quantitative information on the electron inelastic scattering properties in a solid, an analysis of experimental electron spectra based on the extended Landau theory was developed. In this way, the so-called effective energy loss function (EELF) for including both the surface and bulk excitations was obtained [26–28]. Though the EELF enables good agreement between the calculated and experimental REELS spectra, such an EELF is not a pure material property. Since it also relies on the specific experimental condition, it cannot be used in other measurement conditions.

It was assumed that the surface and bulk excitations are two independent events, and the corresponding probabilities can be linearly superimposed in a dielectric functional formulation with the surface and bulk ELFs [29–31]. A simple two-layer model for the interpretation of the measured backscattered electron spectra was first applied. This model was based on the assumption that the sample may be taken as a combination of two independent layers [30,31]: the top three atomic monolayers were characterized with the surface ELF and the others with the bulk ELF. This crude model seems to work for high-energy electrons but not at low energies. Moreover, we note that surface excitations can in fact even happen when electrons are in vacuum and close to the surface.

Tougaard and Chorkendorff [32] developed a method to obtain the differential inverse inelastic mean free path (DIIMFP) from REELS spectra. However, their analysis method considered neither the influence of the angular distribution of elastic scatterings nor the surface effect on the spectra. Hence, these effects cannot be deduced, and the DIIMFP obtained by their method contains not only the bulk excitation but also the surface excitation and partial elastic scattering effect. The calculations of Al [32] and Si [33] show some nonphysical results, in which the DIIMFP has a negative value around $\omega_b + \omega_s$, where ω_b and ω_s are the bulk-plasmon and surface-plasmon excitation energy, respectively. Yubero et al. [34] then improved this calculation by considering the surface effect. They used the trial-and-error procedure to find the best-fitting ELF, but there are still large deviations for the DIIMFP in the energy loss range up to $\omega_b + \omega_s$.

Ding [20,21,35] derived a formulation of the electron inelastic scattering cross section near the surface region via a complex self-energy formula based on a quantum-mechanical approach, where the position- and velocity-dependent DIIMFP contains a dielectric function but is no longer expressed as a simple linear combination of the surface ELF and the bulk ELF. This quantum inelastic scattering model was used in the REELS spectrum simulation for different sample surfaces: Au, Si [36], Ag [37–39], and SiO$_2$ [40]. However, the calculation of this quantum inelastic cross section is quite time-consuming. Therefore, recently a semiclassical model [19] has been frequently used instead. It has been verified that the quantum model and the semiclassical model yield quite similar depth-dependent DIIMFPs in conventional experimental conditions, and there is no significant difference between the REELS spectra simulated by the two models [40].

Werner [41,42] assumed that bulk and surface excitations are uncorrelated. The energy loss distribution of a single

surface effect from REELS spectra was obtained by (i) eliminating the multiple bulk scattering by an iteration formula and (ii) eliminating the elastic peak. Later, Werner [43] considered a more detailed model for describing the generation of REELS to extract the DIIMFPs. An important assumption of Werner's model was that the REELS spectra can be convoluted with terms for various excitations and elastic peak. Novak et al. [44] then used Werner's model to obtain the bulk and surface DIIMFPs from REELS spectra of Ge measured at 1200 and 4000 eV primary electron energies. Using these retrieved DIIMFPs, they achieved excellent agreement between simulated and measured REELS spectra of Ge for 3000 eV.

Werner et al. [45] presented a method to extract the optical constants that is directly related to the ELF from measured REELS spectra. They first decomposed the experimental REELS spectra to obtain the bulk and surface DIIMFPs and found a theoretical expression for bulk and surface DIIMFPs as a function of the parametrized ELF based on dielectric function theory.

Da et al. [11,46] developed a reverse Monte Carlo (RMC) technique to obtain the optical constants of material from the measured REELS spectrum. They used a parametrized ELF to calculate DIIMFP. A simulated REELS spectrum was compared with the experimental one for optimization of the ELF, where a simple linear combination of surface and bulk ELF terms was used for DIIMFP. The simulated annealing method [47] was employed for adjusting the parameter set of the ELF to obtain the best fit. Later Xu et al. [48,49] further improved the RMC method by considering the semiclassical electron inelastic scattering model. The extended RMC method has been successfully applied to various metallic solids [49–52].

When one employs the RMC method to derive the optical constants, the accuracy of the elastic scattering cross section and the inelastic scattering cross section will directly affect the final results. Because silicon and germanium are free-electron-like materials, for which a rather sharp plasmon peak dominates the optical ELF, it is generally difficult to accurately describe both surface and bulk excitations by conventional dielectric function models. In this work, we present a modeling of the electron inelastic scattering cross sections for free-electron-like materials by using the combined full Penn algorithm and the Ritchie-Howie method for the calculation of the bulk excitation cross section and the surface excitation cross section, respectively. Although the improved calculation schema is primarily recommended for free-electron-like materials, it can also be adopted for other materials. We will show that our modeling accurately describes the multiple scattering effects and thereby ensures a high-precision simulation of the REELS spectrum. We apply these inelastic cross sections in our RMC simulation to improve the gained ELF and hence the optical data. With a combination of the high energy resolution REELS measurements and our high-precision RMC method, a high-precision determination of ELFs of silicon and germanium was performed. The refractive index n, the extinction coefficient k, and the complex dielectric function ($\varepsilon = \varepsilon_1 + i\varepsilon_2$) were calculated from these optical ELFs in the energy loss range up to 200 eV. The accuracy of the obtained results is justified by various sum rules.

II. THEORY

A. Reverse Monte Carlo method

The RMC method combines a Monte Carlo modeling of electron transportation for the REELS spectrum simulation with a Markov chain Monte Carlo calculation of the parametrized ELF, $\text{Im}[-1/\varepsilon(q, \omega)]$, where $\varepsilon(q, \omega)$ is the complex dielectric function of the material. The electron-energy loss, ω, corresponds to the photon energy in the optical measurements.

The purpose of the RMC simulation is to find an optimal ELF (or equivalently oscillator parameters), which ensures that the simulated REELS spectrum has the smallest difference with the experimental one. The process of deriving ELF from an experimental REELS spectrum thus becomes a task of global optimization in oscillator parameter space. The simulated annealing method [47], one of the most popular probabilistic searching techniques, is employed for adjusting the parameter set to obtain the best ELF.

In the Monte Carlo simulation of the REELS spectrum, we used the Mott cross section to describe the electron elastic scattering and the dielectric function theory for the description of the electron inelastic scattering processes.

The relativistic representation of the differential elastic cross section, i.e., the Mott differential cross section [53], is

expressed as

$$\frac{d\sigma_e}{d\Omega} = |f(\theta)|^2 + |g(\theta)|^2, \tag{1}$$

where θ is the scattering angle, with scattering amplitudes

$$f(\theta) = \frac{1}{2iK} \sum_l \{(l+1)[\exp(2i\delta_l^+) - 1]$$
$$+ l[\exp(2i\delta_l^-) - 1]\}P_l(\cos\theta), \tag{2}$$

$$g(\theta) = \frac{1}{2iK} \sum_l [\exp(2i\delta_l^-) - \exp(2i\delta_l^+)]P_l^1(\cos\theta), \tag{3}$$

where $P_l(\cos\theta)$ and $P_l^1(\cos\theta)$ are the Legendre and the first-order associated Legendre functions, respectively; δ_l^+ and δ_l^- are spin-up and spin-down phase shifts of the lth partial wave, respectively. The phase shifts are numerically evaluated by solving the Dirac equation for the radial part of the wave function of the scattered electron using the Thomas-Fermi-Dirac atomic potential [54].

A semiclassical model [19] is employed for the electron inelastic scattering process, in which the surface excitation is fully described by the depth-dependent DIIMFP:

$$\sigma(z) = \frac{2}{\pi v^2} \int_{q_-}^{q_+} dq \frac{1}{q} \text{Im}\left[\frac{-1}{\varepsilon(\vec{q}, \omega)}\right]\Theta(-z) + \frac{4\cos\alpha}{\pi^3} \int_{q_-}^{q_+} dq \int_0^{\frac{\pi}{2}} d\theta \int_0^{2\pi} d\phi \frac{q\sin^2\theta \cos(q_\perp z)\exp(q_\parallel z)}{\tilde{\omega}^2 + q_\parallel^2 v_\perp^2}$$
$$\times \left\{\text{Im}\left[\frac{-1}{\varepsilon(\vec{q}_\parallel, \omega) + 1}\right] - \frac{1}{2}\text{Im}\left[\frac{-1}{\varepsilon(\vec{q}_\parallel, \omega)}\right]\right\}\Theta(-z) + \frac{4\cos\alpha}{\pi^3} \int_{q_-}^{q_+} dq \int_0^{\frac{\pi}{2}} d\theta \int_0^{2\pi} d\phi \frac{q\sin^2\theta \exp(-q_\parallel z)}{\tilde{\omega}^2 + q_\parallel^2 v_\perp^2}$$
$$\times \text{Im}\left[\frac{-1}{\varepsilon(\vec{q}_\parallel, \omega) + 1}\right]\left[2\cos\left(\frac{\tilde{\omega}z}{v\cos\alpha}\right) - \exp(-q_\parallel z)\right]\Theta(z) , \qquad v_\perp > 0, \tag{4}$$

and

$$\sigma(z) = \frac{2}{\pi v^2} \int_{q_-}^{q_+} dq \frac{1}{q} \text{Im}\left[\frac{-1}{\varepsilon(\vec{q}, \omega)}\right]\Theta(-z) + \frac{4\cos\alpha}{\pi^3} \int_{q_-}^{q_+} dq \int_0^{\frac{\pi}{2}} d\theta \int_0^{2\pi} d\phi \frac{q\sin^2\theta \cos(-q_\perp z)\exp(-q_\parallel z)}{\tilde{\omega}^2 + q_\parallel^2 v_\perp^2}$$
$$\times \text{Im}\left[\frac{-1}{\varepsilon(\vec{q}_\parallel, \omega) + 1}\right]\Theta(z) + \frac{4\cos\alpha}{\pi^3} \int_{q_-}^{q_+} dq \int_0^{\frac{\pi}{2}} d\theta \int_0^{2\pi} d\phi \frac{q\sin^2\theta \exp(q_\parallel z)}{\tilde{\omega}^2 + q_\parallel^2 v_\perp^2}\left\{\text{Im}\left[\frac{-1}{\varepsilon(\vec{q}_\parallel, \omega) + 1}\right] - \frac{1}{2}\text{Im}\left[\frac{-1}{\varepsilon(\vec{q}_\parallel, \omega)}\right]\right\}$$
$$\times \left[2\cos\left(\frac{\tilde{\omega}z}{v\cos\alpha}\right) - \exp(q_\parallel z)\right]\Theta(-z) , \qquad v_\perp < 0, \tag{5}$$

for an electron penetrating the surface from the solid/vacuum side into the vacuum/solid side, respectively, where $\tilde{\omega} = \omega - qv\sin\theta\cos\phi\sin\alpha$, $q_\parallel = q\sin\theta$, $v_\perp = v\cos\alpha$, and $E = v^2/2$. α is defined as the angle between the surface normal toward the vacuum and the electron moving direction. The upper and lower limits of the integrals are $q_\pm = \sqrt{2E} \pm \sqrt{2(E - \omega)}$. Throughout the paper, atomic units ($e = m = 1$) are used unless stated otherwise.

Differing from a conventional simulation for electron-solid interaction [55,56], this simulation of electron-surface interaction has taken the surface effect, i.e., the inelastic scattering events that occurred in vacuum along an electron trajectory part in approaching and leaving a sample surface, into account. A fast sampling technique [57] is used to determine

the flight length in the Monte Carlo simulation of REELS spectra.

The DIIMFPs in Eqs. (4) and (5) are composed of several terms that depend on depth z, moving direction α, and kinetic energy of the electron E. The first term is due to bulk excitation, which is independent of depth and moving direction and represents the scattering of electrons inside a semi-infinite material, while the remaining terms are for surface excitations. Then, Eqs. (4) and (5) can be written in a short form as [58]

$$\sigma(\omega|E, \alpha, z) = \sigma_{\text{bulk}}(\omega|E, z) + \sigma_{\text{surf}}(\omega|E, \alpha, z). \tag{6}$$

The surface DIIMFP, σ_{surf}, has different expressions when an electron is located at different positions, i.e., in the solid or

vacuum, and in different moving directions, i.e., moving from the solid side into a vacuum or from the vacuum side into the solid. The bulk DIIMFP, σ_{bulk}, can be written according to the electron position as

$$\sigma_{\text{bulk}}(\omega|E, z) = \begin{cases} 0, & z > 0; \\ \sigma'_{\text{bulk}}(\omega|E), & z < 0. \end{cases} \quad (7)$$

The Drude dielectric function in the optical limit, $q = 0$, is written as

$$\varepsilon_D(\omega; \omega_p, \gamma) = 1 - \frac{\omega_p^2}{\omega(\omega + i\gamma)}, \quad (8)$$

where ω_p and γ are the plasmon energy and the damping constant of the plasmon, respectively. In the RMC simulation, a trial optical ELF is parametrized as the sum of N Drude terms as

$$\text{Im}\left[\frac{-1}{\varepsilon(\omega)}\right] = \sum_{i=1}^{N} A_i \text{Im}\left[\frac{-1}{\varepsilon_D(\omega; \omega_{pi}, \gamma_i)}\right], \quad (9)$$

where A_i, ω_{pi}, and γ_i are the oscillator strength, energy, and width of the ith oscillator, respectively, in the $3N$-parameter representation of the optical constants. The function $\text{Re}[-1/\varepsilon(\omega)]$ can be written as

$$\text{Re}\left[\frac{-1}{\varepsilon(\omega)}\right] = \text{Re}\left[\frac{-1}{\varepsilon(0)}\right] + \sum_{i=1}^{N} A_i \text{Re}\left[\frac{-1}{\varepsilon_D(\omega; \omega_{pi}, \gamma_i)}\right]. \quad (10)$$

For conductive materials, the first term, $\text{Re}[-1/\varepsilon(0)]$, has a value of zero. The momentum transfer-dependent ELF, $\text{Im}[-1/\varepsilon(q, \omega)]$, can be extended from the long-wavelength limit, namely from the optical ELF, $\text{Im}[-1/\varepsilon(\omega)] \equiv \text{Im}[-1/\varepsilon(q = 0, \omega)]$, by assuming a dispersion relation.

B. Extension of the ELF

In our previous works [48–52], we used Ritchie and Howie's scheme [24] to extend the momentum transfer-dependent ELF from an optical ELF. The numerical integrations in Eqs. (4) and (5) are easily obtained by using the Ritchie and Howie expression of the ELF because the momentum transfer-dependent ELF is represented as the sum of N Drude-type oscillators in a simple analytical form as

$$\text{Im}\left[\frac{-1}{\varepsilon(q, \omega)}\right] = \sum_{i=1}^{N} A_i \text{Im}\left[\frac{-1}{\varepsilon_D(q, \omega; \omega_{pi}, \gamma_i)}\right], \quad (11)$$

and the function $\text{Re}[-1/\varepsilon(q, \omega)]$ can be expressed as

$$\text{Re}\left[\frac{-1}{\varepsilon(q, \omega)}\right] = B\left(\text{Re}\left[\frac{-1}{\varepsilon(0)}\right], q\right) + \sum_{i=1}^{N} A_i \text{Re}\left[\frac{-1}{\varepsilon_D(q, \omega; \omega_{pi}, \gamma_i)}\right], \quad (12)$$

where B is a function depending on $\text{Re}[-1/\varepsilon(0)]$ and q, and it has a value of 0 for conductive materials. In this work, dealing with semiconductors, we set B as a constant with the value of $\text{Re}[-1/\varepsilon(0)]$. The Drude-type dielectric function assuming a dispersion relation can be written as

$$\varepsilon_D(q, \omega; \omega_{pi}, \gamma_i) = 1 + \frac{\omega_{pi}^2}{\omega_{qi}^2(q, \omega_{pi}) - \omega_{pi}^2 - \omega(\omega + i\gamma_i(q))}, \quad (13)$$

where $\omega_{qi}^2(q, \omega_{pi}) = \omega_{pi}^2 + 2E_F q^2/3 + q^4/4$ describes the plasmon dispersion, and E_F is the Fermi energy. In our previous simulations [48–52], γ_i was taken into account as a constant. In this work, for a more general comparison, a dispersion relation [24] of $\gamma_i(q) = (\gamma_i^2 + q^4/4)^{1/2}$ is used. We note that at $q = 0$, $\omega_{qi} = \omega_{pi}$, so that Eq. (13) is reduced to Eq. (8).

To better distinguish and compare different extension methods of the ELF, the model with setting γ_i as a constant is called the simple Ritchie-Howie method, while the model with a dispersion relation of $\gamma_i(q) = (\gamma_i^2 + q^4/4)^{1/2}$ is called the Ritchie-Howie method. The key function for the determination of the surface DIIMFP term, σ_{surf}, is $\text{Im}[-1/[\varepsilon(q_{\parallel}, \omega) + 1]]$. According to Eqs. (11) and (12), we can calculate the dielectric function $\varepsilon(q_{\parallel}, \omega)$ and derive the functional form of $\text{Im}[-1/[\varepsilon(q_{\parallel}, \omega) + 1]]$.

One of the other scenarios frequently used for the extension of the momentum transfer-dependent ELF from the optical limit into the (q, ω)-plane was proposed by Penn [25], and it will be referred to hereafter as the full Penn algorithm (FPA). Assuming the statistical approximation by neglecting the vertex correction, self-consistency, exchange, and correlation effects, and considering the spherically symmetric charge distribution in the Wigner-Seitz cell, a formula is brought forward to expand the ELF, in terms of the Lindhard ELF, without using any fitting parameters:

$$\text{Im}\left[\frac{-1}{\varepsilon(q, \omega)}\right] = \int_0^{\infty} d\omega_p g(\omega_p) \text{Im}\left[\frac{-1}{\varepsilon_L(q, \omega; \omega_p)}\right], \quad (14)$$

where the expansion coefficient $g(\omega)$ is related to the optical ELF by

$$g(\omega) = \frac{2}{\pi\omega} \text{Im}\left[\frac{-1}{\varepsilon(\omega)}\right], \quad (15)$$

and $\varepsilon_L(q, \omega; \omega_p) = \varepsilon_L^r + i\varepsilon_L^i$ is the Lindhard dielectric function of the free-electron gas with plasmon energy ω_p,

$$\varepsilon_L^r = 1 + \frac{1}{\pi k_F} \frac{1}{Z^2}\left[\frac{1}{2} + \frac{1}{8Z}F\left(Z - \frac{X}{4Z}\right) + \frac{1}{8Z}F\left(Z + \frac{X}{4Z}\right)\right], \quad (16)$$

$$\varepsilon_L^i = \begin{cases} \frac{1}{8k_F} \frac{X}{Z^3}, & 0 \leqslant X \leqslant 4Z(1 - Z); \\ \frac{1}{8k_F} \frac{1}{Z^3}\left[1 - \left(Z - \frac{X}{4Z}\right)^2\right], & |4Z(1 - Z)| \leqslant X \leqslant 4Z(1 + Z); \\ 0, & \text{otherwise,} \end{cases} \quad (17)$$

where $F(x) = (1 - x^2) \ln |(x + 1)/(x - 1)|$, $X = \omega/E_F$, and $Z = q/2k_F$. $E_F = k_F^2/2$ is the Fermi energy and k_F is the Fermi wave vector. They are related to the plasmon energy through the electron density.

Due to the complexity and necessity of the high computation capacity of the FPA method, the single-pole approximation (SPA) was introduced. Applying the SPA in the implementation of the extension of the ELF, the calculations are much simplified [25]. By SPA the Lindhard ELF is written as [25,59]

$$\text{Im}\left[\frac{-1}{\varepsilon_L(q, \omega; \omega_p)}\right] \approx \frac{\pi}{2} \frac{\omega_p^2}{\omega_q} \delta(\omega - \omega_q), \qquad (18)$$

where the plasmon dispersion ω_q is defined by

$$\omega_q^2(\omega_p) = \omega_p^2 + \frac{1}{3} \upsilon_F^2(\omega_p) q^2 + \frac{q^4}{4}, \qquad (19)$$

and $\upsilon_F^2(\omega_p)$ is the Fermi velocity of an electron gas with the plasmon frequency ω_p. The ELF then becomes

$$\text{Im}\left[\frac{-1}{\varepsilon(q, \omega)}\right] \approx \frac{\omega_0}{\omega_q} \text{Im}\left[\frac{-1}{\varepsilon(\omega_0)}\right], \qquad (20)$$

where ω_0 is the solution of the equation $\omega_q(\omega_0) = \omega$.

In Eq. (9), when assuming vanishing damping constants, $\gamma_i \to 0$, and replacing the summation by integration, the Ritchie and Howie's method becomes the SPA. Hence, Ritchie and Howie's method can be regarded as a general SPA method. Of all the extension approaches, the FPA should be more accurate because it contains explicitly both single-electron excitation and plasmon excitation. Mao *et al.* [60] compared the electron inelastic mean free paths (IMFPs) and stopping powers (SPs) calculated by the FPA and SPA methods for Al and Cu, which are representative examples of a free-electron-like material and a non-free-electron-like material, respectively. They found only a small difference between the FPA- and SPA-computed SP and IMFP values for Cu, i.e., non-free-electron-like material. However, for Al a large difference was found between the FPA and SPA calculations of the SP and IMFP at energies below the plasmon energy. We note here that the IMFP is the integrated result of DIIMFP. In other words, with an extension of the ELF by SPA for free-electron-like materials for which a plasmon peak dominates, the single-pole extension of the optical ELF cannot accurately describe the electron inelastic scattering process, especially at low energies. The simulations of energy spectra and secondary electron yields also support the same conclusion, i.e., little difference is found for the results calculated by FPA and SPA for Cu, while the simulation results based on FPA greatly improve the SPA calculation for Al.

Considering the effectiveness of the FPA model for free-electron-like materials, we will use the FPA model to extend the ELF for the calculation of the bulk DIIMFP, σ_{bulk}. However, we will still use the Ritchie-Howie method for the calculation of the surface DIIMFP, σ_{surf}, due to its high efficiency for obtaining the surface energy loss function, $\text{Im}[-1/[\varepsilon(q_\parallel, \omega) + 1]]$. In the following, this combination of the calculation will be referred to as the FPA-Ritchie-Howie method.

We note that for the surface term, σ_{surf}, the Ritchie-Howie method has been improved as compared with the simple Ritchie-Howie method used in our previous work. Using the Ritchie-Howie method is necessary for saving computation time in our RMC simulation. Furthermore, to reduce the surface effect for the extraction of bulk optical data by RMC, we consider employing the experimental REELS spectra measured at high electron energies. In this work, therefore, the experimental REELS spectra of Si and Ge measured at 3000, 4000, and 5000 eV are used.

C. Sum rules

The accuracy of the calculated optical constants, dielectric function, and ELF can be validated by several sum rules [61–63]. In this work, we use them to check the obtained results.

1. The inertial sum rule

It is known that, in addition to the most popular oscillator-strength-sum rule (f-sum rule) for absorption processes, there are companion sum rules for dispersive processes [63]. For example, the refractive index $n(\omega)$ satisfies an inertial sum rule written as

$$R_n(\omega) = \int_0^\omega [n(\omega') - 1] d\omega'. \qquad (21)$$

The theoretical nominal limit value is $R_n(\infty) = 0$. Hence, the conventional definition of relative error, i.e., the percentage error relative to the theoretical value, is invalid. A verification parameter ξ_n can be defined as [61]

$$\xi_n = \frac{\int_0^\infty [n(\omega) - 1] d\omega}{\int_0^\infty |n(\omega) - 1| d\omega}. \qquad (22)$$

The absolute value of ξ_n will be the goodness parameter of the refractive index $n(\omega)$. If the calculated value of ξ_n is less than 2×10^{-3} then it indicates a satisfactory self-consistency [62].

2. The dc-conductivity sum rule

The second consequence of causality and inertia is the dc-conductivity sum rule [61–63],

$$R_{\varepsilon_1}(\omega) = \int_0^\omega [\varepsilon_1(\omega') - 1] d\omega'. \qquad (23)$$

The theoretical limit value is $R_{\varepsilon_1}(\infty) = -2\pi^2 \sigma_0$, where σ_0 is the dc-conductivity. For semiconductors and insulators there are only interband transitions, and the theoretical nominal limit value is $R_{\varepsilon_1}(\infty) = 0$. In this work, we study the optical properties of Si and Ge, both semiconductors. Therefore, we use a similar definition of the verification parameter ξ_{ε_1} for ε_1 as for the case of the inertial sum rule:

$$\xi_{\varepsilon_1} = \frac{\int_0^\infty [\varepsilon_1(\omega) - 1] d\omega}{\int_0^\infty |\varepsilon_1(\omega) - 1| d\omega}. \qquad (24)$$

3. The oscillator-strength sum rule and perfect-screening sum rule

More widely used sum rules are the oscillator-strength sum rule (f-sum rule) and the perfect-screening sum rule (*ps*-sum

rule), which are limiting forms of the Kramers-Kronig integral [64,65]. The f-sum rule for the optical ELF, $\mathrm{Im}[-1/\varepsilon(\omega)]$, the imaginary part of the dielectric function, ε_2, and the extinction coefficient, k, are defined, respectively, as

$$Z_{\mathrm{eff}}|_{\mathrm{ELF}} = \frac{2}{\pi \Omega_p^2} \int_0^\infty \omega \mathrm{Im}[-1/\varepsilon(\omega)] d\omega, \quad (25)$$

$$Z_{\mathrm{eff}}|_{\varepsilon_2} = \frac{2}{\pi \Omega_p^2} \int_0^\infty \omega \varepsilon_2(\omega) d\omega, \quad (26)$$

$$Z_{\mathrm{eff}}|_k = \frac{4}{\pi \Omega_p^2} \int_0^\infty \omega k(\omega) d\omega, \quad (27)$$

where $\Omega_p = \sqrt{4\pi n_a}$, where n_a is the atomic density of the sample. The theoretical values of all three f-sum rules are the atomic number of the element.

The Kramers-Kronig relations lead to the *ps*-sum rule given by [64,65]

$$P_{\mathrm{eff}}|_{\mathrm{ELF}} = \frac{2}{\pi} \int_0^\infty \frac{1}{\omega} \mathrm{Im}[-1/\varepsilon(\omega)] d\omega + \mathrm{Re}[-1/\varepsilon(0)]. \quad (28)$$

For conductors, $\mathrm{Re}[-1/\varepsilon(0)]$ is zero; Eq. (28) then becomes

$$P_{\mathrm{eff}}|_{\mathrm{ELF}} = \frac{2}{\pi} \int_0^\infty \frac{1}{\omega} \mathrm{Im}[-1/\varepsilon(\omega)] d\omega, \quad (29)$$

which is the formula used in our previous works [48–52]. For nonconductors, the refractive index n is much greater than the extinction coefficient k at low frequencies, $\mathrm{Re}[-1/\varepsilon(0)]$ is approximately equal to $1/n^2(0)$, and Eq. (28) becomes

$$P_{\mathrm{eff}}|_{\mathrm{ELF}} = \frac{2}{\pi} \int_0^\infty \frac{1}{\omega} \mathrm{Im}[-1/\varepsilon(\omega)] d\omega + 1/n^2(0). \quad (30)$$

The theoretical value of $P_{\mathrm{eff}}|_{\mathrm{ELF}}$ is a unit. The values of $n(0)$ are set as 3.4155 and 4.0043 for Si and Ge, respectively [63] for the calculation of $P_{\mathrm{eff}}|_{\mathrm{ELF}}$ in Eq. (30).

4. The root-mean-square deviation of the oscillator-strength sum rule

In our previous work on transition metals [52], we proposed a root-mean-square deviation (RMS) of the oscillator-strength sum rule for describing the difference of all three f-sum rules. It is expressed as

$$\mathrm{RMS} = 100 \times \sqrt{\frac{1}{3} \sum_{i=1}^3 \left(\frac{Z_{\mathrm{eff},i} - Z_{\mathrm{eff,mean}}}{Z_{\mathrm{eff,mean}}} \right)^2} \quad (\%), \quad (31)$$

where $Z_{\mathrm{eff},i}$ represents the f-sum rules—$Z_{\mathrm{eff}}|_{\mathrm{ELF}}$, $Z_{\mathrm{eff}}|_{\varepsilon_2}$, and $Z_{\mathrm{eff}}|_k$—and $Z_{\mathrm{eff,mean}}$ is the mean value of the three f-sum rule results. For most materials, the refractive index n is very close to a unit at a photon energy above a few keV. We then have $\mathrm{Im}[-1/\varepsilon] \simeq \varepsilon_2 \simeq 2k$. The integration of three f-sum rules will give almost the same value in this energy loss range. The differences for three f-sum rules come mainly from the low energy loss range. Hence the small RMS value can prove the accuracy of ELF, ε_2, and k in the low-energy-loss range.

III. EXPERIMENT

The high energy resolution REELS measurements of Si and Ge samples were performed at room temperature by using the ESA-31 type electron spectrometer developed in ATOMKI [66]. Before commencement, the measurement surfaces were cleaned by Ar^+ ion sputtering with an ion flux of $120\,\mu A \times \mathrm{min/cm}^2$ at 2 keV kinetic energy. In the REELS measurements, a LEG 62 (VG Microtech) type electron gun was used at a few keV electron energies. The energy width of the elastic peak was around 0.6 eV at full widths at half-maximum, which is coming from the electron energy analyzer caused line broadening and the primary electron beam energy broadening by filament heating (hot cathode tungsten). The scattering angle of θ_0 was 130° using an angular range of $\Delta\theta_0 = \pm 2°$. The angle of the incident electron beam was 50° and the detection angle was 0° with respect to the surface normal. During the REELS measurements, the vacuum in the analysis chamber was better than 3×10^{-9} mbar.

IV. RESULT AND DISCUSSION

A. Comparing models describing the dielectric function

To analyze the differences between the simple Ritchie-Howie, Ritchie-Howie, FPA, and SPA methods in modeling the dielectric function, we performed calculations of the momentum transfer-dependent ELFs of Ge based on these approximations. The optical data of Ge were taken from the measured data [63,67,68]. For the simple Ritchie-Howie model and the Ritchie-Howie model, we need 3N parameters of Drude-type oscillators rather than the specific values of optical ELF as the inputs for the calculation. Hence, fitting the experimental data by Eq. (9) is necessary for further simulation and comparison. Figure 1 shows the optical ELF of Ge obtained from the measured data and the fitting result with Drude-type oscillators.

Figure 2 shows the surface plots of the ELFs obtained by the simple Ritchie-Howie, Ritchie-Howie, FPA, and SPA methods for Ge as a function of momentum transfer and
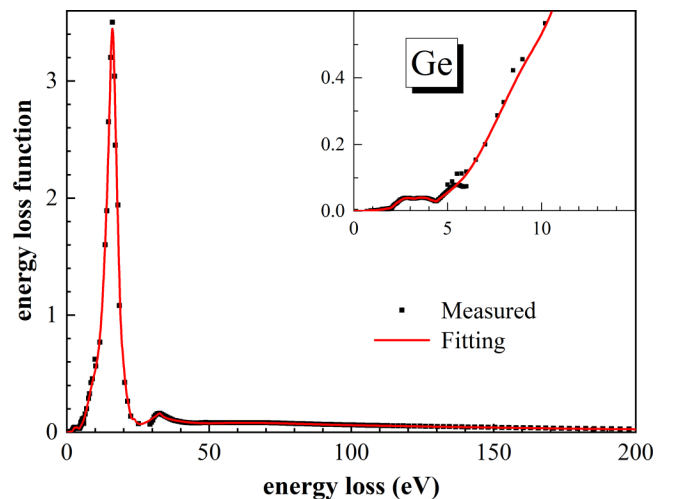
FIG. 1. Comparison of the optical ELF of Ge between the measured data [63,67,68] (squares) with the fitting by Drude-type oscillators.
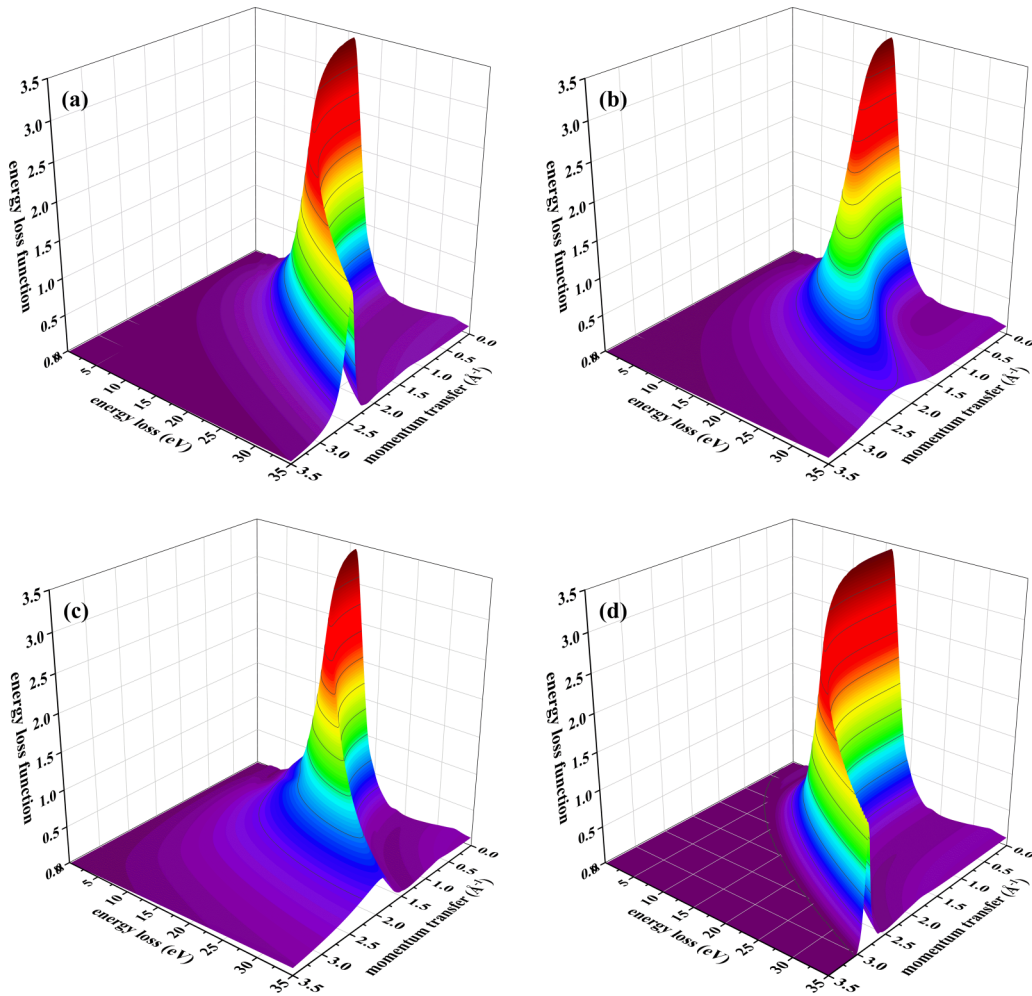
FIG. 2. Surface plots of the energy loss function of Ge as a function of momentum transfer and energy loss, calculated by (a) the simple Ritchie-Howie method, (b) the Ritchie-Howie method, (c) the FPA method, and (d) the SPA method.

energy loss. The differences between the four methods are significant in the region of the large energy losses and high momentum transfers. For Ge, the ELF obtained by the simple Ritchie-Howie method, the Ritchie-Howie method, and the FPA method has a limited but nonzero intensity for a single-particle excitation even for $\omega < \omega_p$. This should be the most important source for the formation of the low-energy secondary electrons. The plasmon excitation intensity in FPA decays quickly when the dispersion enters into the single-particle excitation region [Fig. 2(c)]. SPA, on the other hand, completely ignores the single-electron excitation. This missing contribution is compensated by the intensity of plasmon excitation with a dispersion line that extends up to large q-values, while the ridge height decays very slowly [Fig. 2(d)]. The simple Ritchie-Howie method can give a similar result for plasmon excitation intensity to that of the SPA, i.e., the plasmon excitation intensity decays very slowly, as can be seen in Fig. 2(a). By considering a dispersion relation of γ_i, the Ritchie-Howie method has improved ELF significantly.

Figure 3 shows a detailed comparison of the ELFs of Ge calculated with four extension algorithms at given momentum transfers: 0.1, 0.5, 1.0, and 1.5 Å^{-1}. All the ELFs are calculated from that in the optical limit, i.e., when $q \to 0$. As expected, all algorithms gave almost the same ELFs for the

case of the low momentum transfer as shown in Fig. 3(a). With the increasing momentum transfers, the differences between ELFs obtained by different methods increase. The differences in high-momentum transfer can be attributed to two main reasons. First, the plasmon excitation peaks are located at different positions, which is mainly due to the effect of different plasmon dispersion relations. Second, the plasmon excitation peaks have different intensities, shapes, and peak widths. As discussed above, both in the simple Ritchie-Howie method and SPA, the obtained plasmon excitation intensities are unrealistic. However, taking the dispersion relation of γ_i into account in the Ritchie-Howie method, we can achieve significant improvements for the plasmon excitation intensities and peak widths. However, it is noted that the Ritchie-Howie method leads to only a symmetrical peak feature as seen in Fig. 3(d), which differs from the FPA result. Because the single-electron excitations are completely ignored in SPA, there is no energy loss for the low-energy-loss range for specific momentum transfer, which can be seen in Fig. 3(d). This becomes a serious problem for the description of the low-energy electron inelastic scattering. The simple Ritchie-Howie method, the Ritchie-Howie method, and the FPA method, however, include the single-electron excitations in a certain level.
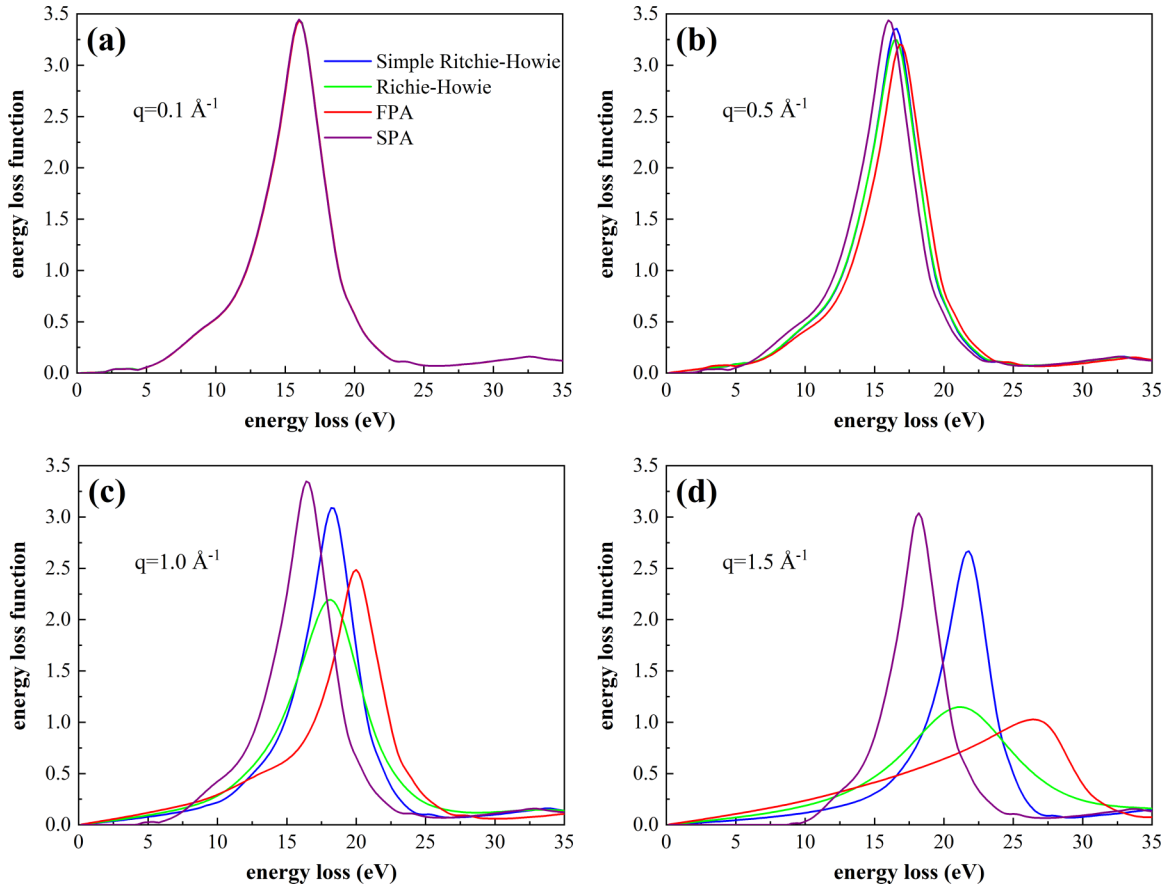
FIG. 3. Comparison of the ELFs of Ge at given momentum transfers as a function of the electron energy loss: (a) $0.1\,\text{Å}^{-1}$, (b) $0.5\,\text{Å}^{-1}$, (c) $1.0\,\text{Å}^{-1}$, and (d) $1.5\,\text{Å}^{-1}$. The ELFs are calculated from the optical ELF by using four different extension algorithms. Blue line: simple Ritchie-Howie method; green line: Ritchie-Howie method; red line: FPA method; purple line: SPA method.

Figure 4 shows a detailed comparison of the ELFs of Ge as a function of the momentum transfer calculated by four extension algorithms at given energy losses: 5, 16, 30, and 50 eV. The ELFs obtained by the SPA method have zero values for large q for a given energy loss. This is due to the limitations of the dispersion relationship in Eq. (19), as will be shown below. For the SPA model, first we obtain a root of the equation of $\omega_q(\omega_0) = \omega$ by solving the following equation:

$$\omega^2 = \omega_0^2 + \frac{1}{3}\upsilon_F^2(\omega_0)q^2 + \frac{q^4}{4}. \qquad (32)$$

Then the q-dependent ELF can be determined according to Eq. (20). Because ω_0^2 is a non-negative value for a given energy loss of ω, Eq. (32) is unsolvable in the range of $q > q_{max}$, where q_{max} can be determined by

$$\frac{1}{3}\upsilon_F^2(\omega_0)q_{max}^2 + \frac{q_{max}^4}{4} - \omega^2 = 0. \qquad (33)$$

Hence, the ELFs obtained by the SPA model will have zero values for large q for a given energy loss. This behavior can also be seen in Figs. 3(c) and 3(d) when the ELF has zero values for small ω values for a given momentum transfer. The simple Ritchie-Howie model gives reasonable results, i.e., it has nonzero values in these regions. Both the simple Ritchie-Howie and SPA models give a very sharp plasmon excitation

peak in the ELF at energy losses of 30 and 50 eV, which proves the phenomenon that the plasmon excitation intensity decays very slowly for the simple Ritchie-Howie and SPA methods. The plasmon excitation peaks are much broader in the Ritchie-Howie and FPA models than in the simple Ritchie-Howie and SPA models as shown in Figs. 4(c) and 4(d).

Shinotsuka *et al.* [69] compared the experimental ELFs of liquid water for several specific momentum transfers with various theoretical results. They found that the FPA method can describe the q-dependent ELF accurately, while there are significant deviations between SPA results and the experimental ELFs. The FPA should be more accurate than other approaches for extension of ELF of free-electron-like materials, which have also been proven in Ref. [60]. From the comparison in Figs. 2, 3, and 4, we can draw the following conclusions: (a) The simple Ritchie-Howie method has a better approximation for electron inelastic scattering than SPA for free-electron-like materials, like Ge. It contains single-particle excitation even for $\omega < \omega_p$. (b) Although there are still deviations, the simple Ritchie-Howie method provides a better approximation for plasmon dispersion than that of SPA. (c) The Ritchie-Howie method is improved compared to the simple Ritchie-Howie method by considering a dispersion relation of γ_i. (d) The q-dependent damping constant in the Ritchie-Howie method can partially improve the broadening effect originated from the single-electron excitation.
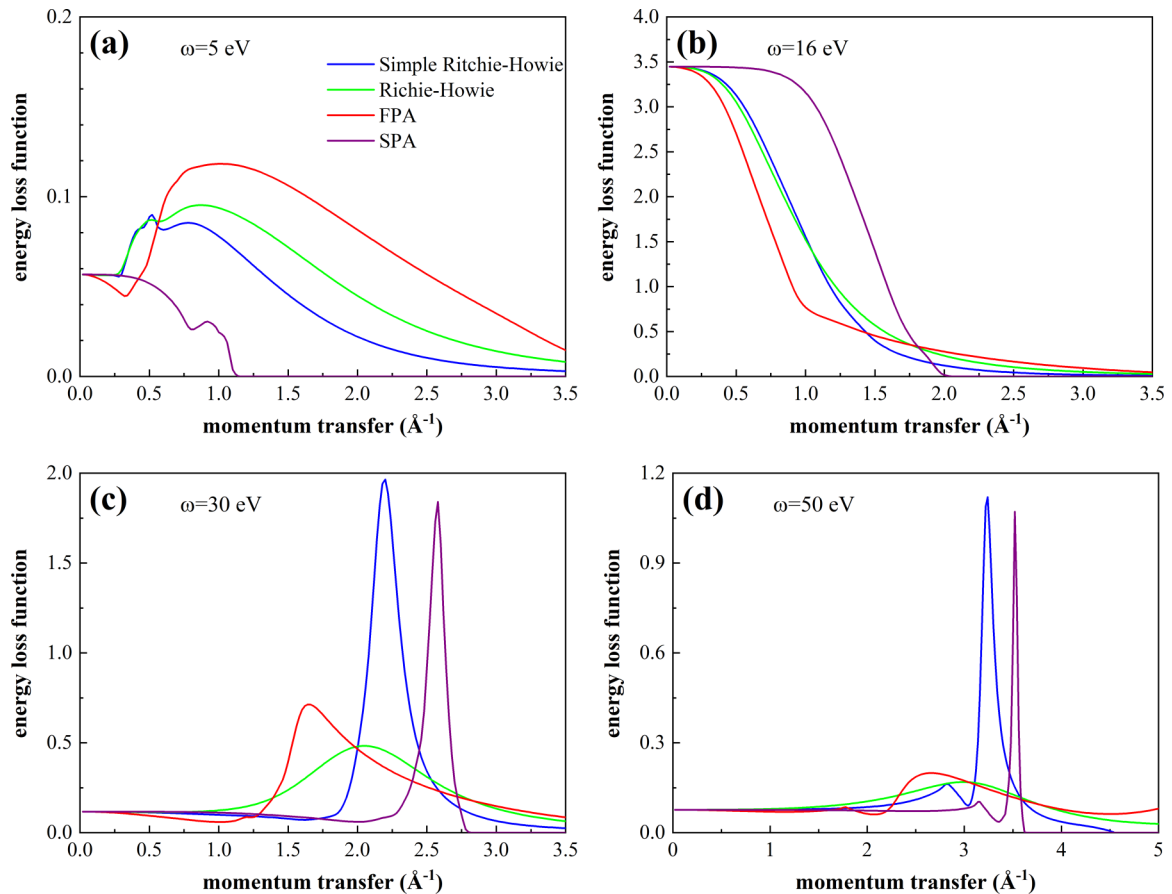
FIG. 4. Comparison of the ELFs of Ge at given energy losses as a function of the momentum transfer: (a) 5 eV, (b) 16 eV, (c) 30 eV, and (d) 50 eV. The ELFs are calculated from the optical ELF by using four different extension algorithms. Blue line: simple Ritchie-Howie method; green line: Ritchie-Howie method; red line: FPA method; purple line: SPA method.

As a result of the previous comparison among the ELFs, the FPA-Ritchie-Howie method is proposed for modeling the inelastic interaction of free-electron-like materials while electrons are crossing a surface region, i.e., using the FPA model for the calculation of the bulk DIIMFP σ_{bulk}, and the Ritchie-Howie method for the surface DIIMFP σ_{surf}. The

Ritchie-Howie method is used due to its high efficiency for obtaining the surface ELF. We note that, as the extraction of the ELF by the RMC method from REELS takes a lot of iteration [46,48], the use of the Ritchie-Howie method for the surface DIIMFP σ_{surf} is a necessary compromising solution for saving computation time in our RMC simulation.
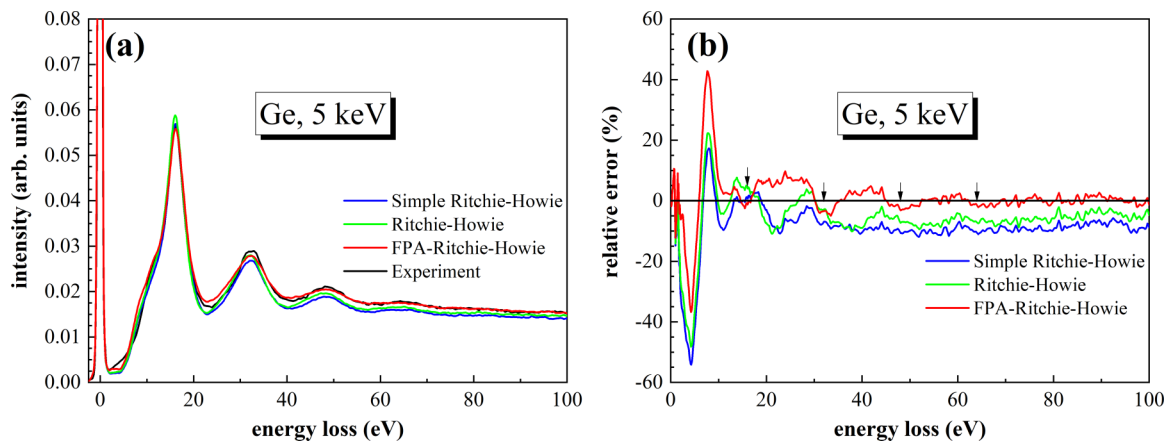
FIG. 5. (a) Comparison of simulated REELS spectra of Ge based on the simple Ritchie-Howie method (blue), the Ritchie-Howie method (green), and the present FPA-Ritchie-Howie method (red) with the experimental REELS spectrum (black) measured at the incident energy of 5000 eV. (b) Comparison of the relative errors between the experimental data and the simulated REELS spectra.
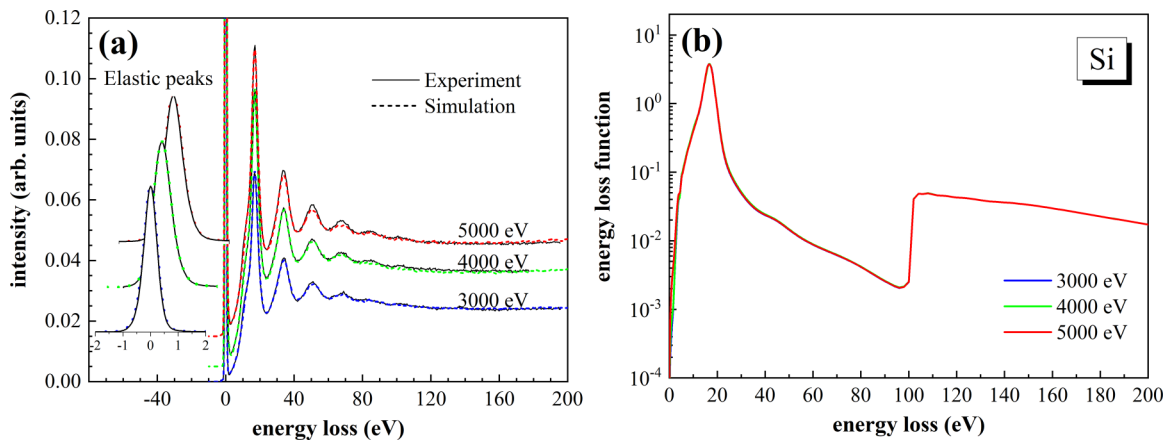
FIG. 6. (a) The final simulated REELS spectra (dash lines) of silicon at 3000, 4000, and 5000 eV, in comparison with experimental results (solid lines). (b) The final ELFs, Im$[-1/\varepsilon(\omega)]$, obtained from the REELS spectra.

B. Verification of the effectiveness of the FPA-Ritchie-Howie method

To check the effectiveness of the FPA-Ritchie-Howie method, we performed simulations of the REELS spectrum of Ge at a primary energy of 5000 eV. As a comparison, the simple Ritchie-Howie method and the Ritchie-Howie method are used to extend the ELF for both bulk DIIMFP and surface DIIMFP, respectively. Figure 5(a) shows a comparison between the REELS spectrum of Ge measured at an incident electron energy of 5 keV and the simulated spectra by these three models, using the optical ELF shown in Fig. 1. To highlight the differences between the experiment and simulations, a relative error has been defined as the difference between the intensities of the simulated REELS spectrum and the experimental one divided by the intensity of the experimental spectrum. Figure 5(b) shows the relative errors, where we mark by arrows four energy losses at 16, 32, 48, and 64 eV, respectively. These energies are the peak positions of the bulk plasmon excitations, i.e., the peak at 16 eV corresponds to the single bulk excitation, and the others are the corresponding multiple-component excitation peaks. The simulated REELS spectrum obtained by the simple Ritchie-Howie method is in good agreement with the experimental data below 20 eV and has almost 10% relative error for energy loss larger than 20 eV. The Ritchie-Howie method gives a similar result with less error in the energy loss range of multiple scattering peaks. In the energy loss range higher than 10 eV, the FPA-Ritchie-Howie method gives the best agreement with the experimental data. It can also be clearly seen from Fig. 5(b) that, while the errors are small for the first plasmon loss peak for all three models used, the FPA-Ritchie-Howie model gives the smallest error for multiplasmon loss peaks as indicated by arrows. From Fig. 5, we can have the same conclusion as before: The simple Ritchie-Howie method cannot give a good description of the electron inelastic scattering for free-electron-like materials. The Ritchie-Howie method has been improved compared to the simple one. The simulated REELS spectrum calculated by the FPA-Ritchie-Howie method is in good agreement with the experimental one. The comparison of REELS spectra proves that the FPA-Ritchie-Howie method can provide a more accurate description of inelastic scattering processes than the

simple Ritchie-Howie method and the Ritchie-Howie method, which is mainly reflected in the agreement of the multiple scattering effect and the intensity of multiple scattering peaks.

The FPA-Ritchie-Howie method is then considered as a high-precision model due to its effectiveness in describing the multiple scattering effect in the Monte Carlo simulation. By using this model in our RMC calculation, the multiple scattering effect can be well deducted and one can obtain the high-precision ELF, which is free from the multiple scattering effect. We note that the simple Ritchie-Howie method was used in our previous works [48–52], and accurate results were obtained. This is the direct consequence of the fact that, with the simple Ritchie-Howie model, similar accuracy can be achieved, as with the FPA method for non-free-electron-like materials. The comparison between SPA and FPA [60] has obtained the same conclusion: that little difference is found between results of the stopping power, IMFP, energy spectra, and secondary electron yields calculated by FPA and SPA for non-free-electron-like material such as Cu. These comparisons also indicate that the multiple scattering effect
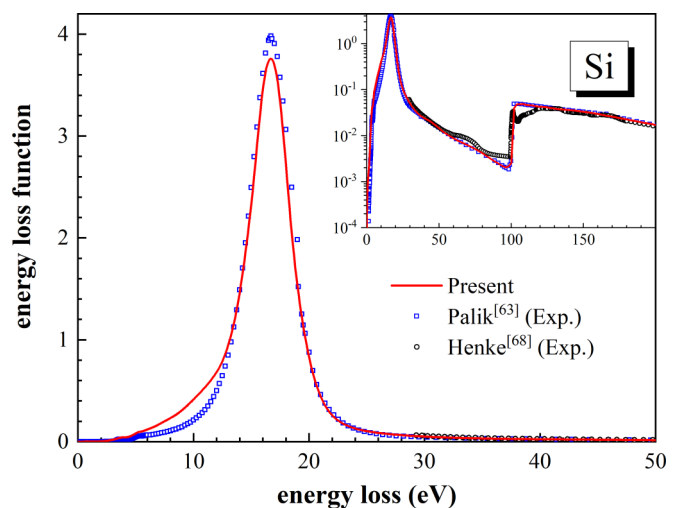
FIG. 7. Comparison of the ELFs between the present data and other sources [63,68] for Si.
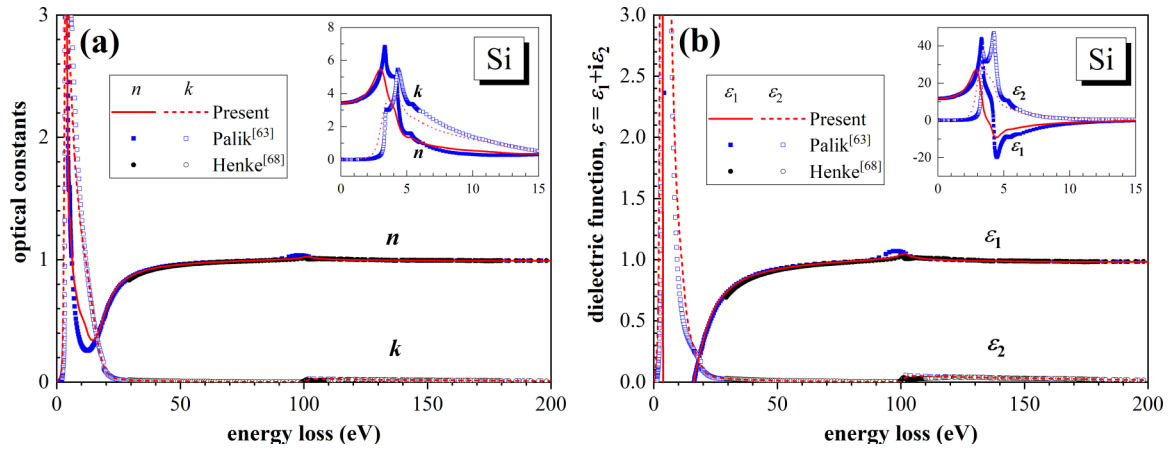
FIG. 8. Comparison of the (a) optical constants and (b) dielectric functions between the present data and other sources [63,68] for Si.

plays a less important role in non-free-electron-like materials compared to free-electron-like materials.

In conclusion, according to the following analysis, we apply the FPA-Ritchie-Howie method for the determination of the momentum transfer-dependent ELF of Si and Ge from the measured REELS using the RMC technique.

1. Si

We have performed the RMC calculations of Si using the FPA-Ritchie-Howie method to determine the ELF from the high energy resolution REELS spectra measured at 3, 4, and 5 keV incident energies. In Fig. 6(a), it is demonstrated that the agreement between the simulated and the experimental REELS spectra of Si for all investigated primary energies is excellent. The ELFs obtained from the experimental spectra are displayed in Fig. 6(b). All ELFs for the three energies have produced REELS spectra in good agreement within the experimental uncertainty. As we can expect, and as is shown in Fig. 6(b), the ELFs obtained from the experimental REELS spectra excited at the primary energies of 3, 4, and 5 keV are almost the same in the whole energy loss region studied.

Figure 7 shows the ELF, averaged over the three energies with a comparison of the data of Palik [63] and Henke [68]. The present ELF is in good agreement with Henke's data above 140 eV. In the energy loss region of higher than 30 eV, the present ELF begins to approach Palik's data and basically coincides with Palik's data near 80 eV. The intensity of the plasmon peak of the present ELF is slightly weaker than that of Palik's data near 17 eV. A distinct difference occurs around 10 eV, where a stronger shoulder in the ELF is obtained by the RMC method. At lower loss energies around a few electron volts, the present ELF rises smoothly without obvious structural features.

The optical constants and dielectric function are determined from the averaged ELF, over three primary energies. Our present optical constants and dielectric function of Si together with the data of Palik [63] and Henke [68] are shown in Fig. 8. A good agreement is shown above 140 eV with Henke's data. The main difference lies in the range of 2–6 eV. There are three peaks in the refractive index n, the extinction coefficient k, and the real and imaginary parts of the dielectric function, ε_1 and ε_2. However, the positions and intensities of the three peaks are different for the present result and Palik's data.
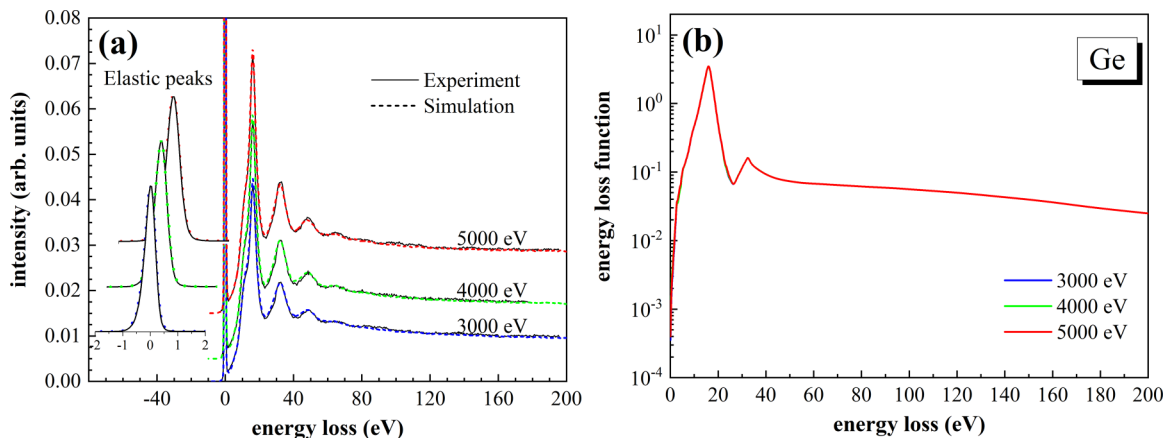
FIG. 9. (a) The final simulated REELS spectra (dash lines) of germanium at 3000, 4000, and 5000 eV, in comparison with experimental results (solid lines). (b) The final ELFs, Im$[-1/\varepsilon(\omega)]$, obtained from the REELS spectra.
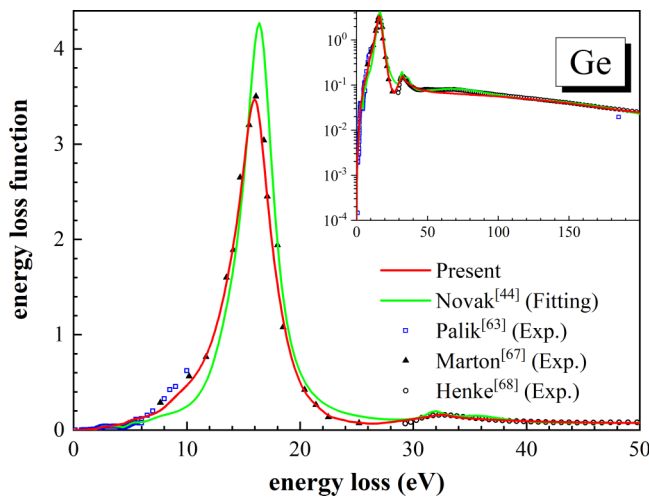
FIG. 10. Comparison on the ELFs between the present data and other sources [44,63,67,68] for Ge.

2. Ge

We have performed the RMC calculations of Ge using the FPA-Ritchie-Howie method to determine the ELF from the high energy resolution REELS spectra measured at 3, 4, and 5 keV incident energies. Figure 9(a) shows that the agreement between the simulated and the experimental REELS spectra of Ge for all three primary energies is excellent. The ELFs obtained from the spectra at each primary energy are displayed in Fig. 9(b). All ELFs for the three energies have produced REELS spectra in good agreement within the experimental uncertainty. ELFs obtained from the experimental REELS spectra excited at the primary energies of 3, 4, and 5 keV are almost the same in the whole energy loss range studied.

Figure 10 shows the ELF averaged over the three energies with a comparison of other experimental data [44,63,67,68]. The present ELF is in good agreement with Henke's data above 100 eV. In the medium energy loss region, the present ELF agrees with Marton's results from reflectance measurements [67]. The present ELF gives slightly smaller values in the energy loss range of 6–12 eV, which will lead to the

reasonable simulation of the REELS spectra at about 8 eV and at 23, 38, and 53 eV. At lower loss energies of less than 6 eV, the present ELF rises smoothly without obvious structural features. Figure 10 also shows a comparison with Novak's results [44] by fitting the imaginary part of the dielectric function from the measured data [63,67,68]. Although the dielectric function is well fitted, there are still significant differences between their ELF and measured data [63,67], which can be seen in Fig. 10. Novak et al. had used their fitting result to perform a quantitative analysis of the plasmon structure of Ge in XPS and Auger spectra.

The averaged ELF is used to determine optical constants and the dielectric function. Figure 11 shows a comparison of our present optical constants and dielectric function of Ge together with Novak's [44] and Henke's [68] data. The present results generally agree well with Novak's data as well as Henke's data in the high energy loss region above 60 eV.

In Figs. 8 and 11, the present data for n and k differ significantly from those of Palik below 6 eV. In the low-energy-loss region below 6 eV, according to Palik's data, there are roughly four peaks in refractive index n, extinction coefficient k, and real and imaginary parts of the dielectric function, ε_1 and ε_2. However, the positions and intensities of the peaks are different between the present result and Palik's data. It should be noted that the RMC is an analytic procedure based on the experimental spectrum. No obvious structure was found in the experimental REELS spectra of Si and Ge below 6 eV. This may be due to several factors. First, there is a strong signal background for the low-energy-loss tail of the surface- and bulk-plasmon peak even down to the energy loss ∼6 eV. Second, the energy resolution of the present REELS spectra still cannot compete with the resolution of HREELS and optical measurements to resolve the low-energy-loss features. Furthermore, electron beam excitation differs from optical excitation for some electronic excitation modes.

Furthermore, to clarify our assumptions, we note that French et al. [70] compared the optical properties of aluminum oxide determined from vacuum ultraviolet spectroscopy and electron energy loss spectroscopy. They found pronounced differences in certain optical properties obtained by optical and electron methods. The differences are considered mainly due to different energy resolution and minor
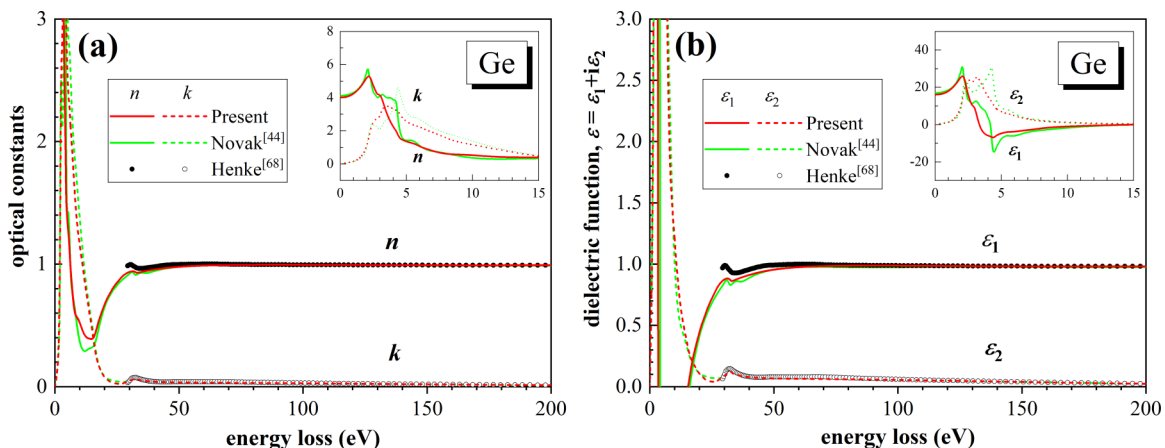
FIG. 11. Comparison of the (a) optical constants and (b) dielectric functions between the present data and other sources [44,68] for Ge.
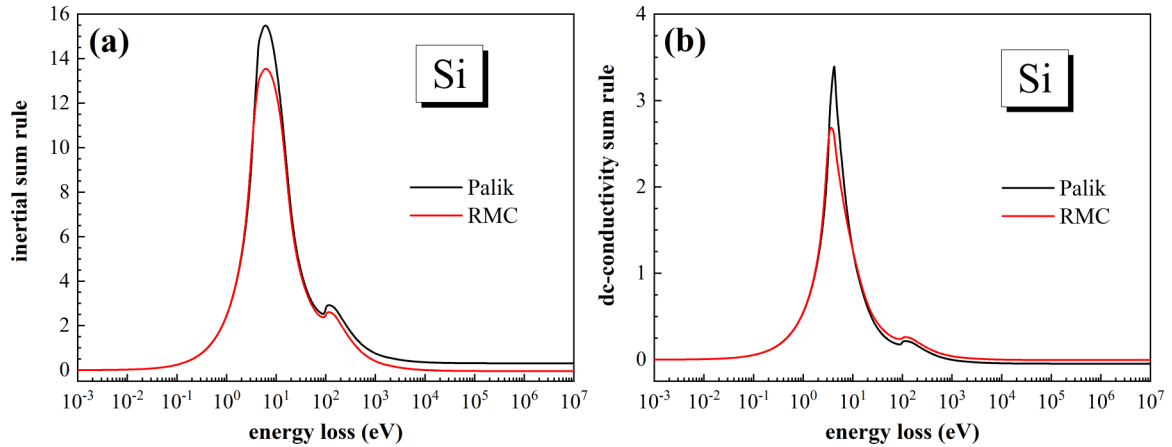
FIG. 12. Inertial sum rule and dc-conductivity sum rule checks of Si in comparison with other source [63].

variations in specimen preparation, data acquisition, or data analysis. Zhang *et al.* [71] investigated the localized surface plasmon modes of a single Ag nanocube for optical and electron excitations in the frame of the discrete dipole approximation. Their comparison between the normalized optical extinction spectrum and electron energy loss spectra (see Fig. 1 in Ref. [71]) shows that electron beam excitation differs from optical excitation, especially in excitation intensity, for some electronic excitation modes.

Although our present ELF data have slightly different fine structure below 6 eV with average values according to the model used in the simulations (FPA-Ritchie-Howie model for a description of the electron inelastic process), the perfect deduction of the multiple scattering effect and the results of various sum rules show that these optical data are the best, with the highest accuracy.

C. Proof of the obtained results by sum rules

Sum rules were used to check the reliability of the present ELF, dielectric function, and optical constants. In the comparison, Henke's data for 200 eV–30 keV [68] and the calculated data by atomic scattering factors for 30 keV–10 MeV [72] are used for the calculation of all the sum rules for the whole dataset. In our present calculations, we set the upper limit of

integration as 10 MeV, which can be considered effectively as infinite for both Si and Ge.

Figure 12 shows the inertial sum rule and dc-conductivity sum rule checks for Si in comparison with Palik's data. Figure 13 shows the inertial sum rule and dc-conductivity sum rule for Ge in comparison with Novak's data. A more detailed numerical comparison is made in Table I.

As can be seen in Table I, all the present inertial sum rule and dc-conductivity sum rule results have an almost ideal value, i.e., zero, for two free-electron-like materials, indicating the high accuracy of the present n and ε_1 data. The verification parameter values for both the inertial sum rule and dc-conductivity sum rule for Si and Ge are less than 1×10^{-3}, also indicating that satisfactory self-consistency has been achieved. For Si, the present results obtained by the RMC method have the best accuracy with verification parameters of -9.626×10^{-4} and -5.084×10^{-4} for ξ_n and ξ_{ε_1}, respectively. The verification parameters ξ_n and ξ_{ε_1} calculated from Palik's data are 9.754×10^{-3} and -6.782×10^{-3}, respectively, one order higher in magnitude compared with our results. This indicates that the values obtained from Palik's data did not meet the requirements of self-consistency judgment proposed in Ref. [62]. For Ge, both the inertial sum rule and the dc-conductivity sum rule for the present results and Novak's data [44] are perfect. We note, however, that our
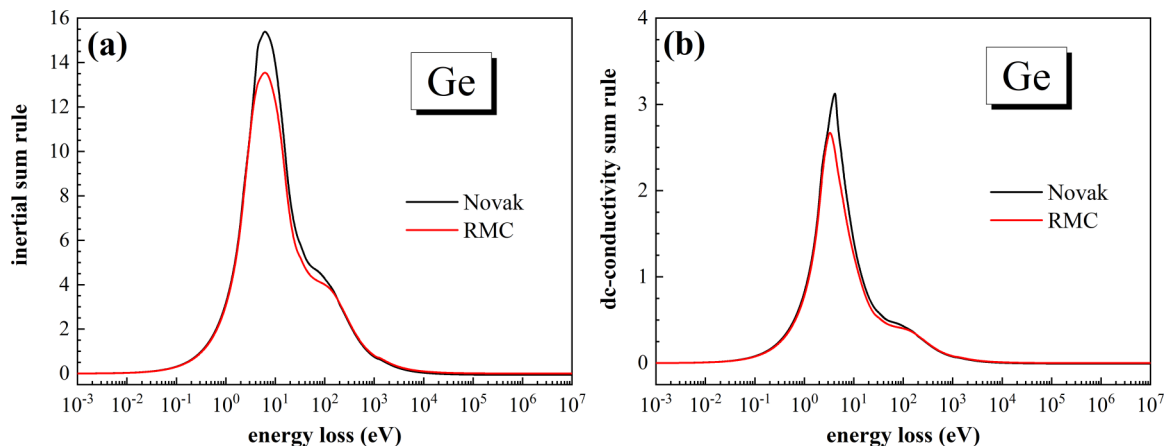
FIG. 13. Inertial sum rule and dc-conductivity sum rule checks of Ge in comparison with other source [44].

TABLE I. List of inertial sum rule and dc-conductivity sum rule checks of Si and Ge.

		$R_n(\infty)$ $(\times 10^{-2})$	ξ_n $(\times 10^{-4})$	$R_{\varepsilon_1}(\infty)$ $(\times 10^{-2})$	ξ_{ε_1} $(\times 10^{-4})$
Si	Present	−4.372	−16.85	−0.453	−8.359
	Palik [63]	30.67	97.54	−4.688	−67.82
Ge	Present	0.183	0.676	0.010	0.195
	Novak *et al.* [44]	−5.854	−19.99	−0.63	−10.07

results have smaller verification parameters ξ_n and ξ_{ε_1} than that of Novak's data [44].

Table II lists the results of f-sum and ps-sum rules of Si and Ge for ELFs. The present ELF for Si has better accuracy with relative errors from the optical measurements being 1.14% and 0.09% for f-sum and ps-sum rules, respectively, as compared to that of Palik's data, 1.82% and −4.09%. For Ge, we also obtained a better ELF using the RMC method. The deviations of the calculated f-sum and ps-sum rules of Ge from the nominal theoretical values are 0.67% and 0.04%, respectively, as compared with 3.87% and 0.52% for Novak's data [44]. There are still some deviations about 0.6–1.2 % from the f-sum rule for both Si and Ge. In our previous work [52], we have discussed similar issues in detail. Given that the ps-sum rule mainly emphasizes the low-energy-loss region of the ELFs and the f-sum rule contains uncertainties from other data sources, the present values are much improved compared with the previous ones. A more detailed comparison can be obtained from the comparison of RMS in Eq. (31).

Table III lists the f-sum rule results for ELFs, ε_2, and k. It is found that Palik's data have a relative error of 1.82% for $Z_{\text{eff}}|_{\text{ELF}}$, a relative error of 3.01% for $Z_{\text{eff}}|_{\varepsilon_2}$, and a relative error of 3.44% for $Z_{\text{eff}}|_k$, showing larger deviation from the theoretical value as compared with our results. The present f-sum rule results, $Z_{\text{eff}}|_{\varepsilon_2}$ and $Z_{\text{eff}}|_k$, are very close to $Z_{\text{eff}}|_{\text{ELF}}$ for both Si and Ge. The small RMS values of 0.027% for Si and 0.010% for Ge in Table III prove the accuracy of the present results again in the low-energy-loss range. The corresponding RMS value from Palik's data of Si is 0.663%, and the corresponding RMS value of Ge from Novak's data is 0.064%.

V. CONCLUSION

The energy loss function of free-electron-like materials is characterized by a very sharp plasmon peak dominating the whole optical energy loss function. This makes the accurate description of the bulk and surface excitations difficult in

TABLE II. List of f-sum and ps-sum rule checks of Si and Ge for ELFs.

		f-sum rule	relative error	ps-sum rule	relative error
Si	Present	14.158	1.13%	1.0011	0.11%
	Palik [63]	14.256	1.82%	0.9591	−4.09%
Ge	Present	32.212	0.66%	1.0004	0.04%
	Novak *et al.* [44]	33.237	3.87%	1.0052	0.52%

TABLE III. List of the f-sum rule checks of Si and Ge for ELF, ε_2, and k.

		ELF	ε_2	k	RMS (%)
Si	Present	14.158	14.146	14.149	0.036
	Palik [63]	14.256	14.421	14.481	0.663
Ge	Present	32.212	32.204	32.206	0.010
	Novak *et al.* [44]	33.237	33.187	33.200	0.064

conventional models. So, the key to the improvement of the description of the energy loss function relies on how accurately we can treat the extension of the energy loss function from the optical limit into the (q, ω) plane. Along these lines, the analysis and comparison of four extension methods, i.e., the simple Ritchie-Howie, Ritchie-Howie, FPA, and SPA methods, have been performed. We found that the simple Ritchie-Howie method has a better approximation for electron inelastic scattering than SPA. It contains the single-particle excitation even for $\omega < \omega_p$. Although there are still deviations, the simple Ritchie-Howie method provides a better approximation for plasmon dispersion than SPA. The Ritchie-Howie method has been improved compared to the simple Ritchie-Howie method by considering a dispersion relation of γ_i. The q-dependent damping constant in the Ritchie-Howie method can improve partially the broadening effect that originates from the single-electron excitation. It was proved, according to our analysis, that the FPA method is the best for the determination of the momentum transfer-dependent ELF for free-electron-like materials. Considering that the Ritchie-Howie method has a natural advantage for obtaining the surface energy loss function, we found that the best model that describes accurately and times efficiently the energy loss function of free-electron-like materials is the combination of FPA with the Ritchie-Howie method. In the so-called FPA-Ritchie-Howie model, the FPA model is used for the calculation of the bulk DIIMFP, and the Ritchie-Howie model is used for the calculation of the surface DIIMFP. The FPA-Ritchie-Howie model has been proved to be a high-precision model, which can accurately describe the multiple scattering effects in the simulation of REELS spectra.

Applying the FPA-Ritchie-Howie model for the determination of the inelastic scattering cross sections, we presented an improved version of the RMC technique to obtain ELF for free-electron-like materials. However, the improved calculation schema is in principle not limited strictly to the free-electron-like materials, as it can also be adopted for other solids. With the combination of the high-accuracy REELS measurements with the high-precision RMC method, the high-precision determination of electron energy loss functions of silicon and germanium from high energy resolution REELS spectra was performed. To reduce the surface effects during the calculations, we used the REELS spectra measured at high energies, i.e., 3, 4, and 5 keV. The refractive index n, the extinction coefficient k, and the complex dielectric function ($\varepsilon = \varepsilon_1 + i\varepsilon_2$) were calculated from these electron-energy loss functions in the energy loss range of 0–200 eV. The high accuracy of the obtained results is justified with the inertial sum rule, the dc-conductivity sum rule, the f-sum rule, and the ps-sum rule. We found that our present optical data of Si

and Ge fulfill the sum rules with an average accuracy of better than 0.11%. Therefore, the previously, either experimentally or theoretically, obtained optical data of these two elements can be replaced with our presently calculated optical data. The use of those data in materials science and surface analysis is highly recommended for further applications describing the properties of Si and Ge.

[1] D. J. Paul, Silicon-germanium strained layer materials in microelectronics, Adv. Mater. **11**, 191 (1999).

[2] C. Claeys and E. Simoen, *Germanium-based Technologies: From Materials to Devices* (Elsevier, Amsterdam, 2011).

[3] S. H. Olsen, A. G. O'Neill, L. S. Driscoll, K. S. K. Kwa, S. Chattopadhyay, A. M. Waite, Y. T. Tang, A. G. R. Evans, D. J. Norris, A. G. Cullis, D. J. Paul, and D. J. Robbins, High-performance nMOSFETs using a novel strained Si/SiGe CMOS architecture, IEEE Trans. Electron. Dev. **50**, 1961 (2003).

[4] Y. Lu, A. Alvarez, C. H. Kao, J. S. Bow, S. Y. Chen, and I. W. Chen, An electronic silicon-based memristor with a high switching uniformity, Nat. Electron. **2**, 66 (2019).

[5] M. E. Castagna, S. Coffa, M. Monaco, L. Caristia, A. Messina, R. Mangano, and C. Bongiorno, Si-based materials and devices for light emission in silicon, Physica E **16**, 547 (2003).

[6] X. Chen, C. Li, and H. K. Tsang, Device engineering for silicon photonics, NPG Asia Mater. **3**, 34 (2011).

[7] P. Chaisakul, D. Marris-Morini, J. Frigerio, D. Chrastina, M. S. Rouifed, S. Cecchi, P. Crozat, G. Isella, and L. Vivien, Integrated germanium optical interconnects on silicon substrates, Nat. Photon. **8**, 482 (2014).

[8] R. Maurand, X. Jehl, D. Kotekar-Patil, A. Corna, H. Bohuslavskyi, R. Laviéville, L. Hutin, S. Barraud, M. Vinet, M. Sanquer, and S. D. Franceschi, A CMOS silicon spin qubit, Nat. Commun. **7**, 13575 (2016).

[9] H. Watzinger, J. Kukučka, L. Vukušić, F. Gao, T. Wang, F. Schäffler, J. J. Zhang, and G. Katsaros, A germanium hole spin qubit, Nat. Commun. **9**, 3902 (2018).

[10] N. W. Hendrickx, D. P. Franke, A. Sammak, M. Kouwenhoven, D. Sabbagh, L. Yeoh, R. Li, M. L. V. Tagliaferri, M. Virgilio, G. Capellini, G. Scappucci, and M. Veldhorst, Gate-controlled quantum dots and superconductivity in planar germanium, Nat. Commun. **9**, 2835 (2018).

[11] B. Da, Y. Sun, S. F. Mao, Z. M. Zhang, H. Jin, H. Yoshikawa, S. Tanuma, and Z. J. Ding, A reverse Monte Carlo method for deriving optical constants of solids from REELS spectra, J. Appl. Phys. **113**, 214303 (2013).

[12] C. J. Powell and J. B. Swan, Origin of the characteristic electron energy losses in aluminum, Phys. Rev. **115**, 869 (1959).

[13] C. J. Powell and J. B. Swan, Origin of the characteristic electron energy losses in magnesium, Phys. Rev. **116**, 81 (1959).

[14] F. Yubero and S. Tougaard, Model for quantitative analysis of reflection-electron-energy-loss spectra, Phys. Rev. B **46**, 2486 (1992).

[15] J. L. Gervasoni and N. R. Arista, Energy loss and plasmon excitation during electron emission in the proximity of a solid surface, Surf. Sci. **260**, 329 (1992).

[16] F. Yubero, J. M. Sanz, B. Ramskov, and S. Tougaard, Model for quantitative analysis of reflection-electron-energy-loss spectra: Angular dependence, Phys. Rev. B **53**, 9719 (1996).

[17] Y. F. Chen and Y. T. Chen, Background removal in surface electron spectroscopy: Influence of surface excitations, Phys. Rev. B **53**, 4980 (1996).

[18] Y. F. Chen and C. M. Kwei, Electron differential inverse mean free path for surface electron spectroscopy, Surf. Sci. **364**, 131 (1996).

[19] Y. C. Li, Y. H. Tu, C. M. Kwei, and C. J. Tung, Influence of the direction of motion on the inelastic interaction between electrons and solid surfaces, Surf. Sci. **589**, 67 (2005).

[20] Z. J. Ding, Self-energy in surface electron spectroscopy: I. Plasmons on a free-electron-material surface, J. Phys.: Condens. Matter **10**, 1733 (1998).

[21] Z. J. Ding, Self-energy in surface electron spectroscopy: II. Surface excitation on real metal surfaces, J. Phys.: Condens. Matter **10**, 1753 (1998).

[22] B. Da, Z. Y. Li, H. C. Chang, S. F. Mao, and Z. J. Ding, A Monte Carlo study of reflection electron energy loss spectroscopy spectrum of a carbon contaminated surface, J. Appl. Phys. **116**, 124307 (2014).

[23] Z. Zheng, B. Da, K. J. Zhang, and Z. J. Ding, Simulation study of electron beam induced surface plasmon excitation at nanoparticles, Chin. J. Chem. Phys. **31**, 655 (2018).

[24] R. H. Ritchie and A. Howie, Electron excitation and the optical potential in electron microscopy, Philos. Mag. **36**, 463 (1977).

[25] D. R. Penn, Electron mean-free-path calculations using a model dielectric function, Phys. Rev. B **35**, 482 (1987).

[26] H. Yoshikawa, R. Shimizu, and Z. J. Ding, Energy loss functions derived by Monte Carlo simulation from the Au 4f XPS spectrum, Surf. Sci. **261**, 403 (1992).

[27] T. Nagotomi, Z. J. Ding, and R. Shimizu, Derivation of new energy-loss functions as applied to analysis of Si 2p XPS spectra, Surf. Sci. **359**, 163 (1996).

[28] Z. M. Zhang, Z. J. Ding, H. M. Li, K. Tökési, D. Varga, and J. Tóth, Effective energy loss function of silver derived from reflection electron energy loss spectra, Surf. Interface Anal. **38**, 632 (2006).

[29] F. Yubero and S. Tougaard, Quantitative analysis of reflection electron energy-loss spectra, Surf. Interface Anal. **19**, 269 (1992).

[30] K. Tőkési, D. Varga, L. Köver, and T. Mukoyama, Monte Carlo modelling of the backscattered electron spectra of silver at the 200 eV and 2 keV primary electron energies, J. Electron Spectrosc. Relat. Phenom. **76**, 427 (1995).

[31] K. Tőkési, L. Kövér, D. Varga, J. Tóth, and T. Mukoyama, Effects of surface loss in REELS spectra of silver, Surf. Rev. Lett. **04**, 955 (1997).

[32] S. Tougaard and I. Chorkendorff, Differential inelastic electron scattering cross sections from experimental reflection electron-energy-loss spectra: Application to background removal in electron spectroscopy, Phys. Rev. B **35**, 6570 (1987).

[33] S. Tougaard and J. Kraaer, Inelastic-electron-scattering cross sections for Si, Cu, Ag, Au, Ti, Fe, and Pd, Phys. Rev. B **43**, 1651 (1991).

[34] F. Yubero, S. Tougaard, E. Elizalde, and J. M. Sanz, Dielectric loss function of Si and SiO2 from quantitative analysis of REELS spectra, Surf. Interface Anal. **20**, 719 (1993).

[35] Z. J. Ding, Inelastic scattering of electrons at real metal surfaces, Phys. Rev. B **55**, 9999 (1997).

[36] Z. J. Ding and R. Shimizu, Monte Carlo simulation study of reflection-electron-energy-loss-spectroscopy spectrum, Phys. Rev. B **61**, 14128 (2000).

[37] Z. J. Ding, H. M. Li, Q. R. Pu, Z. M. Zhang, and R. Shimizu, Reflection electron energy loss spectrum of surface plasmon excitation of Ag: A Monte Carlo study, Phys. Rev. B **66**, 085411 (2002).

[38] Z. J. Ding, K. Salma, H. M. Li, Z. M. Zhang, K. Tokesi, D. Varga, J. Toth, K. Goto, and R. Shimizu, Monte Carlo simulation study of electron interaction with solids and surfaces, Surf. Interface Anal. **38**, 657 (2006).

[39] K. Salma, Z. J. Ding, Z. M. Zhang, P. Zhang, K. Tokesi, D. Varga, and J. Toth, Quantification of surface effects: Monte Carlo simulation of REELS spectra to obtain surface excitation parameter, Surf. Sci. **603**, 1236 (2009).

[40] B. Da, S. F. Mao, and Z. J. Ding, Validity of the semi-classical approach for calculation of the surface excitation parameter, J. Phys.: Condens. Matter **23**, 395003 (2011).

[41] W. S. M. Werner, Surface and bulk plasmon coupling observed in reflection electron energy loss spectra, Surf. Sci. **526**, L159 (2003).

[42] W. S. M. Werner, C. Eisenmenger-Sittner, J. Zemek, and P. Jiricek, Scattering angle dependence of the surface excitation probability in reflection electron energy loss spectra, Phys. Rev. B **67**, 155412 (2003).

[43] W. S. M. Werner, Differential surface and volume excitation probability of medium-energy electrons in solids, Phys. Rev. B **74**, 075421 (2006).

[44] M. Novák, L. Kövér, S. Egri, I. Cserny, J. Tóth, D. Varga, and W. Drube, A simple statistical model for quantitative analysis of plasmon structures in XPS and Auger spectra of free-electron-like materials, J. Electron. Spectrosc. Relat. Phenom. **163**, 7 (2008).

[45] W. S. M. Werner, K. Glantschnig, and C. Ambrosch-Draxl, Optical constants and inelastic electron-scattering data for 17 elemental metals, J. Phys. Chem. Ref. Data **38**, 1013 (2009).

[46] B. Da, S. F. Mao, Y. Sun, and Z. J. Ding, A new analytical method in surface electron spectroscopy: Reverse Monte Carlo method, e-J. Surf. Sci. Nanotech. **10**, 441 (2012).

[47] S. Kirkpatrick, C. D. Gelatt, and M. P. Vecchi, Optimization by simulated annealing, Science **220**, 671 (1983).

[48] H. Xu, B. Da, J. Tóth, K. Tőkési, and Z. J. Ding, Absolute determination of optical constants by reflection electron energy loss spectroscopy spectra, Phys. Rev. B **95**, 195417 (2017).

[49] H. Xu, L. H. Yang, B. Da, J. Tóth, K. Tőkési, and Z. J. Ding, Study of optical and electronic properties of nickel from reflection electron energy loss spectra, Nucl. Instrum. Methods Phys. Res. B **406**, 475 (2017).

[50] H. Xu, L. H. Yang, J. Tóth, K. Tőkési, B. Da, and Z. J. Ding, Absolute determination of optical constants of three transition metals using reflection electron energy loss spectroscopy, J. Appl. Phys. **123**, 043306 (2018).

[51] L. H. Yang, M. Menyhard, A. Sulyok, K. Tőkési, and Z. J. Ding, Optical properties and excitation energies of iridium derived from reflection electron energy loss spectroscopy spectra, Appl. Surf. Sci. **456**, 999 (2018).

[52] L. H. Yang, K. Tőkési, B. Da, and Z. J. Ding, Determination of electron inelastic mean free path of three transition metals from reflection electron energy loss spectroscopy spectrum measurement data, Eur. Phys. J. D **73**, 21 (2019).

[53] N. F. Mott, The scattering of fast electrons by atomic nuclei, Proc. R. Soc. London A **124**, 425 (1929).

[54] R. A. Bonham and T. G. Strand, Analytical expressions for potentials of neutral Thomas-Fermi-Dirac atoms and for the corresponding atomic scattering factors for x rays and electrons, J. Chem. Phys. **39**, 2200 (1963).

[55] R. Shimizu and Z. J. Ding, Monte Carlo modeling of electron-solid interactions, Rep. Prog. Phys. **55**, 487 (1992).

[56] Z. J. Ding and R. Shimizu, A Monte Carlo modeling of electron interaction with solids including cascade secondary electron production, Scanning **18**, 92 (1996).

[57] W. A. Coleman, Mathematical verification of a certain Monte Carlo sampling technique and applications of the technique to radiation transport problems, Nucl. Sci. Eng. **32**, 76 (1968).

[58] J. M. Gong, L. H. Yang, K. Tőkési, and Z. J. Ding, Surface and bulk excitations of silver determined from the reflected energy loss spectroscopy spectra, Eur. Phys. J. D **73**, 24 (2019).

[59] Z. J. Ding and R. Shimizu, Inelastic collisions of kV electrons in solids, Surf. Sci. **222**, 313 (1989).

[60] S. F. Mao, Y. G. Li, R. G. Zeng, and Z. J. Ding, Electron inelastic scattering and secondary electron emission calculated without the single pole approximation, J. Appl. Phys. **104**, 114907 (2008).

[61] M. Altarelli and D. Y. Smith, Superconvergence and sum rules for the optical constants: Physical meaning, comparison with experiment, and generalization, Phys. Rev. B **9**, 1290 (1974).

[62] E. Shiles, T. Sasaki, M. Inokuti, and D. Y. Smith, Self-consistency and sum-rule tests in the Kramers-Kronig analysis of optical data: Applications to aluminum, Phys. Rev. B **22**, 1612 (1980).

[63] E. D. Palik, *Handbook of Optical Constants of Solids* (Academic, New York, 1991), Vol. 2.

[64] Y. Sun, H. Xu, B. Da, S. F. Mao, and Z. J. Ding, Calculations of energy-loss function for 26 materials, Chin. J. Chem. Phys. **29**, 663 (2016).

[65] S. Tanuma, C. J. Powell, and D. R. Penn, Use of sum rules on the energy-loss function for the evaluation of experimental optical data, J. Electron Spectrosc. Relat. Phenom. **62**, 95 (1993).

[66] L. Kövér, D. Varga, I. Cserny, J. Tóth, and K. Tökési, Some applications of high-energy, high-resolution Auger electron spectroscopy using bremsstrahlung radiation, Surf. Interface Anal. **19**, 9 (1992).

[67] L. Marton and J. Toots, Optical properties of germanium in the far ultraviolet, Phys. Rev. **160**, 602 (1967).

[68] B. L. Henke, E. M. Gullikson, and J. C. Davis, X-ray interactions: Photoabsorption, scattering, transmission, and reflection at E = 50–30,000 eV, Z = 1–92, At. Data Nucl. Data Tables **54**, 181 (1993).

[69] H. Shinotsuka, B. Da, S. Tanuma, H. Yoshikawa, C. J. Powell, and D. R. Penn, Calculations of electron inelastic mean free paths. XI. Data for liquid water for energies from 50 eV to 30 keV, Surf. Interface Anal. **49**, 238 (2017).

[70] R. H. French, H. Müllejans, and D. J. Jones, Optical properties of aluminum oxide: Determined from vacuum ultraviolet and electron energy-loss spectroscopies, J. Am. Ceram. Soc. **81**, 2549 (1998).

[71] K. J. Zhang, B. Da, and Z. J. Ding, LSP modes of Ag nanocube and dimer studied by DDA simulation, Surf. Interface Anal. **48**, 1256 (2016).

[72] D. E. Cullen, J. H. Hubbell, and L. Kissel, *EPDL97: The Evaluated Data Library, 1997 Version* (Lawrence Livermore National Lab., Livermore, CA,1997).